# Atomic force microscopy measurements of anionic liposomes reveal the effect of liposomal rigidity on antigen-specific regulatory T cell responses

Benne, N.; Leboux, R.J.T.; Glandrup, M.; Duijn, J. van; Lozano Vigario, F.; Neustrup, M.A.; ... ; Slütter, B.

Journal of Controlled Release 318 (2020) 246–255

Contents lists available at ScienceDirect

Journal of Controlled Release

journal homepage: www.elsevier.com/locate/jconrel

# Atomic force microscopy measurements of anionic liposomes reveal the effect of liposomal rigidity on antigen-specific regulatory T cell responses

Naomi Benne[a], Romain J.T. Leboux[a], Marco Glandrup[a], Janine van Duijn[a], Fernando Lozano Vigario[a], Malene Aaby Neustrup[a], Stefan Romeijn[a], Federica Galli[b], Johan Kuiper[a], Wim Jiskoot[a], Bram Slütter[a,*]

[a] Division of BioTherapeutics, Leiden Academic Centre for Drug Research, Leiden, the Netherlands
[b] Leiden Institute of Physics, Leiden, the Netherlands

ARTICLE INFO

*Keywords:*
Liposomes
Atomic force microscopy
Rigidity
Regulatory T cells
Tolerance

ABSTRACT

Regulatory T cells (Tregs) are vital for maintaining a balanced immune response and their dysfunction is often associated with auto-immune disorders. We have previously shown that antigen-loaded anionic liposomes composed of phosphatidylcholine (PC) and phosphatidylglycerol (PG) and cholesterol can induce strong antigen-specific Treg responses. We hypothesized that altering the rigidity of these liposomes while maintaining their size and surface charge would affect their capability of inducing Treg responses. The rigidity of liposomes is affected in part by the length and saturation of carbon chains of the phospholipids in the bilayer, and in part by the presence of cholesterol. We used atomic force microscopy (AFM) to measure the rigidity of anionic $OVA_{323}$-containing liposomes composed of different types of PC and PG, with or without cholesterol, in a molar ratio of 4:1(:2) distearoyl (DS)PC:DSPG (Young's modulus (YM) 3611 ± 1271 kPa), DSPC:DSPG:CHOL (1498 ± 531 kPa), DSPC:dipalmitoyl (DP)PG:CHOL (1208 ± 538), DPPC:DPPG:CHOL (1195 ± 348 kPa), DSPC:dioleoyl (DO)PG:CHOL (825 ± 307 kPa), DOPC:DOPG:CHOL (911 ± 447 kPa), and DOPC:DOPG (494 ± 365 kPa). Next, we assessed if rigidity affects the association of liposomes to bone marrow-derived dendritic cells (BMDCs) *in vitro*. Aside from DOPC:DOPG liposomes, we observed a positive correlation between liposomal rigidity and cellular association. Finally, we show that rigidity positively correlates with Treg responses *in vitro* in murine DCs and *in vivo* in mice. Our findings underline the suitability of AFM to measure liposome rigidity and the importance of this parameter when designing liposomes as a vaccine delivery system.

## 1. Introduction

Regulatory T cells (Tregs) are important for the resolution of inflammation after infection, immune suppression, and immune homeostasis [1]. They do so by producing anti-inflammatory cytokines [2], consuming pro-inflammatory interleukin 2 (IL-2) and interrupting effector T cell metabolism [3]. A reduction in the number or the dysfunction of Tregs has been implicated in many diseases, including type 1 diabetes, rheumatoid arthritis, and multiple sclerosis [4]. Due to their immunosuppressive capacity, inducing Tregs is an attractive approach for immunotherapy in inflammatory and auto-immune diseases. Approaches to induce tolerance include oral administration of disease-

*Abbreviations:* ACK, ammonium-chloride-potassium; AFM, atomic force microscopy; APC, antigen-presenting cell; APTES, (3-aminopropyl)triethoxysilane; cIMDM, complete Iscove's Modified Dulbecco's Medium; cRPMI 1640, complete Roswell Park Memorial Institute Medium; DC, dendritic cell; DDA, dimethyldioctadecylammonium; DIC, N,N'-diisopropylcarbodiimide; DLS, dynamic light scattering; DMF, dimethylformamide; DODA, dimethyldioleoylammonium; DOPC, 1,2-dioleoyl-sn-glycero-3-phosphocholine; DOPG, 1,2-dioleoyl-sn-glycero-3- phosphoglycerol; DPPC, 1,2-dipalmitoyl-sn-glycero-3-phosphocholine; DPPE-Rho, 1,2-dipalmitoyl-sn-glycero-3-phosphoethanolamine-N-(lissamine rhodamine B sulfonyl); DPPG, 1,2-dipalmitoyl-sn-glycero-3- phosphoglycerol; DSC, differential scanning calorimetry; DSPC, 1,2-distearoyl-sn-glycero-3-phosphocholine; DSPG, 1,2-distearoyl-sn-glycero-3-phosphoglycerol; FCS, fetal calf serum; FOXP3, forkhead box P3; FTIR, Fourier-transform infrared spectroscopy; GM-CSF, granulocyte-macrophage colony-stimulating factor; i.v., intravenous; IL, interleukin; LE, loading efficiency; MHC, major histocompatibility complex; NTA, nanoparticle tracking analysis; PB, phosphate buffer; PBS, phosphate-buffered saline; PC, phosphatidylcholine; PDI, polydispersity index; PG, phosphatidylglycerol; QI, quantitative imaging; RMS, root mean square; SEM, scanning electron microscopy; TDB, trehalose 6,6'-dibehenate; TFA, trifluoracetic acid; TGF, transforming growth factor; Th, T helper; Tm, transition temperature; Treg, regulatory T cell; WT, wild-type; YM, Young's modulus

* Corresponding author at: Einsteinweg 55, 2333 CC, Leiden, the Netherlands.
*E-mail address:* b.a.slutter@lacdr.leidenuniv.nl (B. Slütter).

https://doi.org/10.1016/j.jconrel.2019.12.003
Received 25 October 2019; Received in revised form 3 December 2019; Accepted 4 December 2019
Available online 05 December 2019

specific antigens [5], as well as the use of tolerogenic nanoparticles (reviewed by Kishimoto and Maldonado [6]). Many of these tolerogenic nanoparticles co-encapsulate antigens with ligands to enhance tolerance or inhibit effector responses, such as CD22 [7] or rapamycin [8,9], respectively. However, it is possible to use "bare" particles that exploit natural tolerogenic processes, generally by targeting scavenger receptors [10]. When using such nanoparticles, their physicochemical properties determine their efficiency to induce antigen-specific Treg responses. For instance, cationic particles are superior to anionic particles when comparing the efficiency of their association to APCs, as well as induction of pro-inflammatory responses [11], whereas we and other groups have shown that anionic nanoparticles like PG-containing liposomes are more efficient at inducing tolerance [12,13]. Besides the surface charge, particle size has also been shown to affect liposome-APC interactions and subsequent induction of antigen-specific Tregs. For example, nano-sized particles are taken up more efficiently by APCs than micron-sized particles, leading to stronger APC activation and subsequent immune responses [14]. Finally, the rigidity of nanoparticles is another important parameter for the induction of T cell responses [15,16], however, to our knowledge, it is unknown whether Treg responses are similarly affected by this parameter. The rigidity of a particle, expressed here as YM, describes the deformation of an entire particle and is not the same as the intrinsic deformation property of the material(s) that the particle is made of. Rigid particles were previously shown to be more efficiently taken up by macrophages compared to soft particles [17], and rigid liposomes were able to induce stronger DC activation *in vivo* [18]. Furthermore, rigid liposomes led to higher levels of antigen presentation on MHC-II in DCs [19]. Finally, increasing liposomal rigidity has been shown to result in increased humoral and cellular immune responses [20–22].

Here, we aimed to study the relationship between liposomal rigidity and induced antigen-specific Treg responses. Liposomal rigidity is related to, but not the same as, the rigidity of the lipid bilayer. Bilayer rigidity is strongly dependent on the transition temperature ($T_m$) of the constituent phospholipids. Below the $T_m$, phospholipid bilayers are in a relatively rigid gel state, whereas above the Tm they are in a (much less rigid) liquid disordered state [23]. Analytical techniques such as differential scanning calorimetry (DSC) [24] are commonly used to determine the average Tm of liposomal bilayers. However, these techniques do not measure the absolute rigidity of bilayers, let alone of liposomal particles. Moreover, bilayers containing substantial amounts of cholesterol (CHOL) lack a clear Tm [25], making the use of these analytical techniques less useful. In the present study, we employed atomic force microscopy (AFM), as this technique allows for simultaneous imaging and rigidity measurement of individual liposomes, whether or not they contain CHOL [26]. Here we present an AFM-based method to measure the YM of a range of anionic liposomes, by immobilizing them on (3-aminopropyl)triethoxysilane (APTES)-modified silicon plates. Moreover, we show that liposomal rigidity is positively correlated with Treg responses against a loaded antigen *in vitro* and *in vivo*.

## 2. Materials and methods

### 2.1. Materials

The phospholipids 1,2-distearoyl-sn-glycero-3-phosphocholine (DSPC), 1,2-dipalmitoyl-sn-glycero-3-phosphocholine (DPPC), 1,2-dioleoyl-sn-glycero-3-phosphocholine (DOPC), 1,2-distearoyl-sn-glycero-3-phosphoglycerol (DSPG), 1,2-dipalmitoyl-sn-glycero-3- phosphoglycerol (DPPG), 1,2-dioleoyl-sn-glycero-3- phosphoglycerol (DOPG), and 1,2-dipalmitoyl-sn-glycero-3-phosphoethanolamine-N-(lissamine rhodamine B sulfonyl) (DPPE-Rho) were purchased from Avanti Polar Lipids (Alabaster, AL, USA). Cholesterol (CHOL), APTES, acetic acid, N,N′-diisopropyl carbodiimide (DIC), and triisopropyl silane were purchased from Sigma-Aldrich (Zwijndrecht, the Netherlands). The ovalbumin-derived peptide $OVA_{323}$ (ISQAVHAAHAEINEAGR) was purchased from Invivogen (San Diego, California, USA). Tentagel R-RAM resin was purchased from Rapp Polymere (Tübingen, Germany). Amino acids were supplied by Novabiochem (Merck, Darmstadt, Germany). Dimethylformamide (DMF), trifluoracetic acid (TFA), piperidine, pyridine, and acetonitrile were purchased from Biosolve (Valkenswaard, the Netherlands). Oxyma was supplied by Carl Roth (Karlsruhe, Germany). DCM was purchased from Honeywell (Fisher, Landsmeer, the Netherlands). Diethyl ether was acquired from VWR (Amsterdam, the Netherlands). Polycarbonate track-etched membranes with a pore size of 400 nm and 200 nm were obtained from Millipore (Kent, UK).

For cell culture, $Ca^{2+}$- and $Mg^{2+}$-free phosphate-buffered saline (PBS), Iscove's Modified Dulbecco's Medium (IMDM), Roswell Park Memorial Institute Medium (RPMI 1640), L-glutamine, and penicillin/streptomycin were purchased from Lonza (Basel, Switzerland). Fetal calf serum (FCS) was purchased from PAA Laboratories (Ontario, Canada). β-mercaptoethanol was purchased from Sigma-Aldrich (Zwijndrecht, the Netherlands). Granulocyte-macrophage colony-stimulating factor (GM-CSF) was purchased from PeptroTech (London, UK).

The antibodies CD45.1-PE-Dazzle594 (A20), Thy1.2-PE-Cy7 (53–2.1), Gata-3-PE (16E10A23), T-bet-APC (4B10), IL-17A-AF488 (TC11-18H10.1), and CD11c-PerCP-Cy5.5 (N418) were purchased from Biolegend (CA, USA). FOXP3-eFluor450 (FJK-16S), CD25-AF488 (PC61.5), Ki-67-FITC (SolA15), fixable viability dye-APC-eFluor780, IL-10-PerCP-Cy5.5 (JES5-16E3), IFNγ-APC (XMG1.2), and FOXP3/transcription factor staining kit were purchased from eBioscience (Thermofisher Scientific, MA, USA). CD4-V500 (RM4–5) was purchased from BD Biosciences (CA, USA).

### 2.2. Methods

#### 2.2.1. Preparation of $OVA_{323}$-AF488

The $OVA_{323}$ peptide with the sequence ISQAVHAAHAEINEAGRGC was synthesized using a Liberty Blue microwave-assisted peptide synthesizer. Synthesis was performed on a 0.1 mmol scale with a low-loading (0.18 mmol/g) Tentagel® R-RAM resin. Amino acid activation was performed using DIC as the activator and oxyma as a base, and Fmoc-deprotection was performed with 20% piperidine in DMF. The resin was washed five times with DMF and five times with dichloromethane. To protect the N-terminal amine, the peptide was reacted with 5% *v*/v acetic acid anhydride and 6% pyridine *v*/v in DMF for 1 h at room temperature. Subsequently, cleavage from the resin was performed using a mixture of TFA:triisopropyl silane:water, 38/1/1 *v*/v/v. The peptide was precipitated using ice-cold diethyl ether. The precipitate was collected by centrifugation before resuspension in water:acetonitrile 4/1 v/v, after which the acetonitrile was evaporated and the remaining aqueous solution was lyophilized overnight. Purification was performed by RP-HPLC on a Kinetic Evo C18 column with a Shimadzu system comprising two LC-8A pumps and an SPD-10AVP UV–Vis detector. The collected fractions were analyzed using LC-MS and pure fractions were pooled, the organic solvent was evaporated and the peptide solution was lyophilized overnight. To obtain fluorescently labeled $OVA_{323}$, the peptide was incubated for 48 h at 4 °C with AlexaFluor 488 $C_5$ maleimide (ThermoFisher Scientific, Landsmeer, Netherlands) at pH 7.4 (100 mM HEPES buffer). The purified fluorescent peptide was obtained by RP-HPLC and mass was confirmed by LC-MS.

#### 2.2.2. Liposome preparation

Liposomes were prepared using the thin film dehydration-rehydration method, as described previously [27]. Briefly, phospholipids with or without CHOL (10 mg/mL, 1 mL) were dissolved in chloroform and mixed in a 50 mL round-bottom flask at a molar ratio of 4:1(:2) PC:PG(:CHOL). The chloroform was evaporated under vacuum in a

rotary evaporator (Rotavapor R-210, Büchi, Switzerland) for 1 h at 40 °C. The resulting lipid film was rehydrated with 250 μg $OVA_{323}$ dissolved in 1 mL Milli-Q water and homogenized using glass beads. The liposome dispersion was snap-frozen in liquid nitrogen, followed by freeze-drying overnight (Christ alpha 1–2 freeze-dryer, Osterode, Germany). The freeze-dried lipid cake was slowly rehydrated using 10 mM sodium phosphate buffer (PB), pH 7.4. Two volumes of 500 μL and one volume of 1000 μL PB were successively added, with intervals of 30 min between each addition. The mixture was vortexed well between each hydration step, and the resulting dispersion was left to rehydrate for at least 1 h. The multilamellar vesicles were sized by high-pressure extrusion (LIPEX Extruder, Northern Lipids Inc., Canada) by passing the dispersion four times through stacked 400-nm and 200-nm pore size membranes (Whatman® NucleporeTM, GE Healthcare, Little Chalfont, UK). The resulting liposomes were assumed to be unilamellar. Homogenization, rehydration, and extrusion were performed at a temperature above the $T_m$ of the phospholipids. To separate non-encapsulated $OVA_{323}$ from the liposomes, liposomes were washed in a Vivaspin 2 centrifuge membrane concentrator (MWCO 300 kDa, Sartorius, Göttingen, Germany) by centrifugation at 524 *g* and 4 °C. To prepare fluorescently labeled liposomes, 0.1 mol% of PC was replaced with DPPE-Rho. To prepare liposomes with fluorescently labeled $OVA_{323}$, 10% of the $OVA_{323}$ was replaced with $OVA_{323}$-AF488. Liposomes were stored at 4 °C and used for further experiments within 2 weeks.

#### 2.2.3. Liposome characterization

The *Z*-average diameter and polydispersity index (PDI) of the liposomes were measured by dynamic light scattering (DLS) using a NanoZS Zetasizer (Malvern Ltd., Malvern, UK). The same instrument was used to measure ζ-potential by laser Doppler electrophoresis. The liposomes were diluted 100-fold in PB to a total volume of 1 mL for these measurements. Particle concentration was measured using nanoparticle tracking analysis (NTA), as described previously [28], for optimal AFM measurements. Liposomes were diluted in PB to a particle concentration between $10^7$ and $10^9$ particles/mL based on the DLS attenuation. NTA measurements were performed using a NanoSight LM20 (NanoSight, Amesbury, UK). Capture time was 60 s, the camera shutter was set to 1500 ms, and gain to 680. To determine the concentration of loaded $OVA_{323}$, the peptide was extracted from liposomes using a modified Bligh-Dyer method, as described previously [29]. Briefly, 100 μL of aqueous liposomal dispersion or a known concentration of free peptide as control was mixed with 250 μL methanol and 125 μL chloroform and vortexed. Then, 250 μL of 0.1 M HCl and 125 μL chloroform were added and the mixture was vortexed and subsequently centrifuged for 5 min at 524 *g* to separate the two phases. The upper phase was collected and analyzed by RP- UPLC. Sample injections were 10 μL and the column used was a 1.7 μm BEH C18 column (2.1 × 50 mm, Waters ACQUITY UPLC, Waters, MA, USA). Column and sample temperatures were 40 °C and 4 °C, respectively. The mobile phases were Milli-Q water with 0.1% TFA (solvent A) and acetonitrile with 0.1% TFA (solvent B). For separation, the mobile phases were applied in a linear gradient from 5% to 95% solvent B over 5 min at a flow rate of 0.370 mL/min. Peptides were detected by absorbance at 214 nm using an ACQUITY UPLC TUV detector (Waters ACQUITY UPLC, Waters, MA, USA).

#### 2.2.4. Preparation of APTES-modified silicon plates

To allow for imaging of anionic liposomes, (negatively charged) silicon plates were modified with APTES, to obtain a positively charged surface, as described previously [30]. Briefly, the plates were washed with acetone and methanol and dried in a vacuum oven (Binder, Germany) for 30 min at 50 °C. The plates were incubated in a solution of 3/7 *v*/v $H_2O_2/H_2SO_4$ at 120 °C to remove any organic contaminants and to hydroxylize the silicon surface. The plates were then washed with water and dried for 30 min in a vacuum oven. The plates were incubated overnight in 2% v/v APTES in toluene, washed thoroughly with toluene to remove any excess APTES, and subsequently washed with methanol, and dried in a vacuum oven at 175 °C. Lastly, a curing step for the hydrolysis of residual ethoxy groups was performed at 120 °C for 30 min followed by incubation in Milli-Q water at 40 °C for 2 h after which the plates were washed with methanol and stored in a vacuum oven at 175 °C until use. The smoothness of the APTES-modified plates was confirmed using AFM in QI mode. A sharp cantilever (Oltespa, Opus, Bulgaria) with a nominal spring constant of 2 N/m, a nominal resonance frequency of 70 kHz and a tip radius of < 7 nm was used to image the surface of the plates. The sample tilt was corrected using the JPK Data Processing software v6.1.79 flattening function. Images were extracted using Gwyddion v2.50 and the heights of structures on the plates were determined. The roughness of the plates was expressed as root mean square (RMS) [31], and plates used had RMS values between 0.6 and 3 nm, which was deemed to have minimal interference and to favor adsorption of liposomes [32].

#### 2.2.5. Sample preparation for AFM measurements

APTES-modified plates were attached to glass microscope slides using Reprorubber® (Thin Pour Kit, Flexbar Machine Corporation, USA). A small glass ring with a diameter of 15 mm and a height of 3 mm was attached on the plate to form a small basin. Next, 200 μL of liposomal formulation (particle concentrations of about $10^{12}$–$10^{13}$ particles/mL, as measured by NTA) was applied to the plate and incubated at room temperature for 5 min. The plate was gently washed with PB without exposure of the plate to air to remove free liposomes.

#### 2.2.6. Scanning electron microscopy (SEM) of cantilevers

The cantilever tip radius of the HSC-20 cantilever (Team Nanotec, Germany) was assessed by SEM using an FEI Nova nanoSEM 200. Imaging was performed in high vacuum mode at 15 kV and a spot of 4.0 at a tilt of 45°. Images were captured at 200,000-fold magnification and the radius of the cantilever tip was determined using the SEM software.

#### 2.2.7. AFM measurements

To image the liposomes a JPK Nanowizard 3 (JPK Instruments AG, Berlin, Germany) was used. Measurements were performed at 25 ± 1 °C in QI mode. The AFM probe used was a Team Nanotec (Germany) HSC-20 hemispherical cone-shaped tip cantilever with gold-reflective coating and metal carbide coating on the tip side, with a nominal spring constant of 0.2 N/m, a nominal resonance frequency of 15 kHz and a tip radius of 35 nm, as determined by SEM. The cantilever was calibrated using contact-based calibration and thermal tuning. For calibration, the setpoint was 0.1 V on approach with a dynamic baseline. Imaging of the liposomes was performed with a z-length 200 nm and a set point between 0.5 and 0.85 nN. The area of the image was 2 × 2 μm at a resolution of 128 × 128 pixels with a pixel rate of 20 msec/pixel. Scan line artifacts were removed, line fitting was applied to the images, and sample tilt was corrected. Liposomes with a height below 40 nm were excluded from analysis to prevent interference from the substrate. Force *vs.* height curves were measured for each pixel of the AFM image. After subtracting the cantilever deflection, the force *vs.* tip-sample separation (or distance) curves were fitted using the Hertz/Sneddon model [33] for a hemispherical cantilever tip according to the following equation [34]:

$$F = \frac{4\sqrt{R}}{3}\frac{E}{1-\nu^2}\delta^{\frac{3}{2}} \quad (1)$$

where F is the force as measured by AFM, R is the tip radius as measured by SEM, E is the YM, $\nu$ is Poisson's ratio, set to 0.5 for soft materials such as liposomes [35], and δ is the indentation of the sample, also measured by AFM. The YM was determined for the center of the liposomes.

Raw data images and force *vs.* height curves were processed using JPK Data Processing software v6.1.70. Data from the images were extracted using Gwyddion v2.50. Between 31 and 450 liposomes were

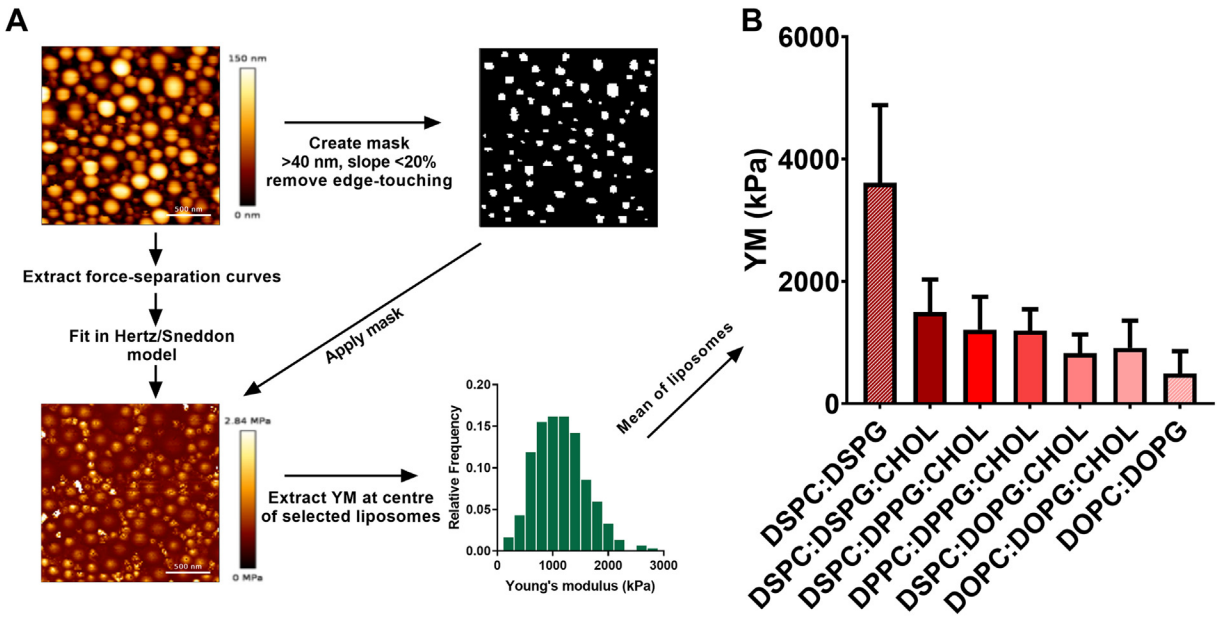


**Fig. 1.** AFM measurements of liposomes. (A) Schematic overview of the AFM method used to determine the rigidity of liposomes. Liposomes were immobilized on APTES-modified silicon plates. The rigidity of the liposomes was measured using AFM in QI mode. AFM images were processed in JPK data processing software v6.1.70. Scan line artifacts were removed and images were corrected for baseline tilt. YM data per pixel was extracted by fitting each force-separation curve with the Hertz/Sneddon model resulting in a YM map. To remove the interference of the silicon substrate, a mask was created in Gwyddion 2.50, selecting a threshold of 40 nm with a slope of < 20%. Liposomes touching the edges of the image were not included in the analysis. This mask was applied to the YM map, and YM data was extracted for each liposome. Only the center of each liposome was used to calculate the mean YM per formulation. Representative AFM images of DSPC:DPPG:CHOL liposomes. (B) Rigidity, expressed as YM, of the different liposomes. Data shown is mean values ± SD, $n$ = 31–450. Significant differences as measured by one-way ANOVA are displayed in Table S3.

analyzed per formulation (Fig. 1.A).

### 2.2.8. BMDC culture

Bone marrow was isolated from the tibias and femurs of wild-type (WT) C57BL/6 mice. A single-cell suspension of bone marrow cells was obtained by straining over a 70 μm cell strainer (Greiner Bio-One B.V., Alphen aan den Rijn, NL). Cells were cultured for 10 days in complete IMDM (cIMDM) which contains IMDM supplemented with 2 mM L-glutamine, 8% *v*/v FCS, 100 U/mL penicillin/streptomycin, and 50 μM β-mercaptoethanol at 37 °C and 5% $CO_2$ in 95-mm Petri dishes (Greiner Bio-One B.V., Alphen aan den Rijn, NL) and 20 ng/mL GM-CSF. The medium was refreshed every other day.

### 2.2.9. Liposome or antigen association to BMDCs

BMDCs were cultured as described above. After 10 days of culture, BMDCs were plated in F-bottom 96-well plates (Greiner Bio-One B.V., Alphen aan den Rijn, Netherlands) at 50,000 cells/well. To measure association (either by uptake or adsorption) of liposomes to BMDCs, liposomes prepared with 0.1 mol% Rho-DPPE or controls (non-fluorescent liposomes or medium) were added at a concentration of 20 μg/mL lipids in supplemented IMDM. To measure $OVA_{323}$ association to DCs, liposomes encapsulating fluorescently labeled $OVA_{323}$ were added to a concentration of 0.1 μg/mL $OVA_{323}$. Cells were incubated for 4 h at 37 °C and 5% $CO_2$. Subsequently, excess liposomes were removed by washing the cells several times with cIMDM, and cells were incubated overnight. Cells were stained with a fluorescent antibody against CD11c-PerCP-Cy5.5 (N418) and fixable viability dye-APC-eFluor780 and subsequently analyzed by flow cytometry (CytoFLEX S, Beckman Coulter, CA, USA). The presence of the fluorescent label in DCs indicated the association of either liposomes or peptide by BMDCs. Data were analyzed with FlowJo software V10 (Treestar, OR, USA).

### 2.2.10. In vitro Treg induction by liposome-pulsed BMDCs

BMDCs were cultured as described above, plated to 50,000 cell/well in a 96-well F-bottom plate, and pulsed for 4 h with liposomes or controls in cIMDM. Spleens from OT-II mice were strained through a 70 μm cell strainer to obtain a single-cell suspension. Erythrocytes were lysed using ammonium-chloride-potassium (ACK) lysis buffer (0.15 M $NH_4Cl$, 1 mM $KHCO_3$, 0.1 mM $Na_2EDTA$

pH 7.3). $CD4^+$ T cells were isolated using a $CD4^+$ T cell isolation kit (Miltenyi Biotec B.V., Leiden, Netherlands) according to the manufacturer's protocol. After exposure, BMDCs were washed with cIMDM to remove free liposomes, and 100,000 $CD4^+$ T cells/well were added to the BMDCs. Co-cultures were incubated for 72 h in RPMI 1640 medium supplemented with 2 mM L-glutamine, 10% *v*/v FCS, 100 U/mL penicillin/streptomycin, and 50 μM β-mercaptoethanol. Cells were stained for Thy1.2-PE-Cy7, CD4-V500, viability-APC-eFluor780, FOXP3-eFluor450, and Ki-67-FITC, and analyzed by flow cytometry (CytoFLEX S, Beckman Coulter, CA, USA). Data were analyzed using FlowJo software V10 (Treestar, OR, USA).

### 2.2.11. Animals

C57BL/6 and OT-II transgenic mice on a C57BL/6 background were purchased from Jackson Laboratory (CA, USA), bred in-house under standard laboratory conditions, and provided with food and water *ad libitum*. All animal work was performed in compliance with the Dutch government guidelines and the Directive 2010/63/EU of the European Parliament. Experiments were approved by the Ethics Committee for Animal Experiments of Leiden University.

### 2.2.12. Adoptive transfer

Eleven-week-old female C57BL/6 mice were randomized into 4 groups based on weight. On day 0, all mice received 500,000 $CD45.1^+CD4^+$ T cells splenocytes isolated from a female OT-II transgenic mouse *via* the tail vein. On day 1, mice were immunized intravenously (i.v.) with a single injection of DSPC:DSPG, DSPC:DSPG:CHOL, DOPC:DOPG or DOPC:DOPG:CHOL liposomes containing 1 nmol $OVA_{323}$ in PBS, in a total volume of 200 μL *via* the tail

vein. On day nine, mice were sacrificed by cervical dislocation and spleens were immediately removed. Spleens were processed as mentioned above and stained for CD4-V500, CD45.1-PE-Dazzle594, Thy1.2-PE-Cy7, viability-APC-eFluor780, CD25-AF488, Gata-3-PE, T-bet-APC, and FOXP3-eFluor450 and measured by flow cytometry (CytoFLEX S, Beckman Coulter, CA, USA). To measure cytokine production, splenocytes were stimulated *ex vivo* with $OVA_{323}$ (10 μg/mL). After 1 h brefeldin A (3 μg/mL) was added and cells were incubated for a further 5 h. Cells were subsequently stained for CD4-V500, CD45.1-PE-Dazzle594, Thy1.2-PE-Cy7, viability-APC-eFluor780, IFNγ-APC, IL-17A-AF 488, and IL-10-PerCP-Cy5.5, and analyzed by flow cytometry. Data were analyzed using FlowJo software V10 (Treestar, OR, USA).

#### 2.2.13. Statistical analysis

Results were analyzed using one-way or two-way ANOVA, followed by Bonferroni's multiple comparisons test and was performed using GraphPad Prism version 8.1.1 for Windows (GraphPad Software, CA, USA).

## 3. Results

### 3.1. Preparation of liposomes

Tregs are vital for maintaining immune homeostasis and are an attractive target for immunotherapy. We have previously demonstrated that liposomes prepared with DSPC, DSPG and CHOL in a molar ratio of 4:1:2 and loaded with an initial $OVA_{323}$ concentration of 250 μg/mL induce strong antigen-specific Treg responses. In order to assess how the rigidity of these liposomes affects the Treg responses, we altered the rigidity of the liposomes by using phospholipids with different carbon chain-lengths (*e.g.* DSPC, di-18:0 PC *vs.* DPPC, di-16:0 PC), unsaturation in the lipid chain (*e.g.* DSPC, di-18:0 PC *vs.* DOPC, di-18:1 (Δ9-Cis) PC) or exclusion of CHOL (Table S1). The resulting liposomes were between 138 and 177 nm in size (Table 1). Exclusion of CHOL slightly, but significantly, reduced the size of the liposomes ($p < .05$). All formulations were monodisperse, indicated by a PDI of about 0.1. As expected, because of the incorporation of an anionic PG phospholipid, all liposomes had a negative ζ-potential. The loading efficiency (LE) of the $OVA_{323}$ was between 11.4 and 24.6%.

### 3.2. Effect of lipid composition on liposome rigidity

To study the effect of lipid composition on the rigidity of the liposomes, we measured the YM of the anionic liposomes by AFM. Liposomes were successfully immobilized on APTES-modified silicon plates and were imaged in quantitative imaging (QI) mode (Fig. 1 and Table S2). AFM confirmed the size and monodispersity measured by dynamic light scattering and allowed extraction of force-separation curves and determination of the YM of single liposomes (Fig. 1A). The most rigid liposomes were DSPC:DSPG liposomes, while the least rigid liposomes were DOPC:DOPG liposomes (Fig. 1B). This was expected, since DSPC:DSPG bilayers are in a gel state, and DOPC:DOPG bilayers are in a liquid disordered state at 25 °C (Table 1). For DSPC:DSPG liposomes, the addition of CHOL significantly reduced the YM (from 3611 ± 1271 kPa to 1498 ± 530 kPa, $p < .001$), while this was reversed for DOPC:DOPG liposomes (from 493 ± 365 kPa to 911 ± 447 kPa, $p = .0153$). Interestingly, we observed that replacing a small amount of a high-$T_m$ phospholipid with a lower-$T_m$ phospholipid has the same effect as replacing all phospholipids by a lower-$T_m$ one. For instance, both DSPC:DPPG:CHOL (YM = 1159 ± 525 kPa), where DSPC has a higher $T_m$ than DPPC, and DPPC:DPPG:CHOL liposomes (YM = 1211 ± 399 kPa) were significantly less rigid than DSPC:DSPG:CHOL liposomes (YM = 1498 ± 531 $p < .005$), while not being significantly different from each other ($p > .99$). A similar effect was observed for DSPC:DOPG:CHOL and DOPC:DOPG:CHOL liposomes. Finally, we found that the $T_m$ values and the molar ratio of the constituent lipids do not significantly correlate with the rigidity of the liposomes (Fig. S1).

### 3.3. Effect of liposomal composition on liposome association to BMDCs and Treg responses in vitro

Next, we assessed how the rigidity of liposomes affects the uptake by APCs and the induction of Tregs by the APCs. To this end, we incorporated a fluorescently labeled phospholipid, Rho-DPPE, into the lipid bilayer and exposed BMDCs for 4 h to these formulations (Fig. 2A). For almost all formulations, we observed a positive trend between liposomal rigidity and association. Interestingly, the highest association was observed for the least rigid, DOPC:DOPG liposomes. It should be noted, however, that the DOPC:DOPG liposomes showed primarily passive association, indicated by high cell association at 4 °C (Fig. 2B), while all other liposomes showed negligible association at 4 °C (Fig. S2). Furthermore, DOPC:DOPG liposomes did not appear to effectively deliver their cargo

while the association of DSPC:DSPG liposomes led to a significant 7.5-fold increase in $OVA_{323}$ association compared to free $OVA_{323}$ (control), both DOPC:DOPG:CHOL and DOPC:DOPG liposomes did not increase $OVA_{323}$ association compared to the control (Fig. 2C).

To determine whether the liposomal composition affected Treg responses, BMDCs were pulsed with liposomes for 4 h, and subsequently co-cultured with OT-II $CD4^+$ T cells. After three days of incubation, induced Tregs were identified using flow cytometry (Fig. 3A, B, and C). Among all tested $OVA_{323}$-containing liposomes, the DSPC:DSPG liposomes induced the strongest Treg responses, with a 1.6-fold increase in % $FOXP3^+$ population in live $CD4^+Ki\text{-}67^+$ T cell population compared to free $OVA_{323}$. Also DSPC:DSPG, DSPC:DSPG:CHOL, DSPC:DPPG:CHOL, and DPPC:DPPG:CHOL liposomes showed significantly higher Treg responses compared to free $OVA_{323}$. Furthermore, we observed a significant correlation between the liposomal rigidity (determined by AFM) and Treg responses (Fig. 3D). Interestingly, there was no clear relationship between the association of liposomes with BMDCs and subsequent Treg responses (Fig. 3E).

### 3.4. Effect of liposomal composition on Treg response in vivo

Next, we aimed to assess whether liposome rigidity affects Treg

**Table 1**
Physicochemical characteristics of liposomal formulations.

| Lipid composition (molar ratio) | *Z*-average ± SD (nm) | PDI ± SD | ζ-potential ± SD (mV) | LE (%)[a] | Phase state at room temperature |
|---|---|---|---|---|---|
| DSPC:DSPG:CHOL (4:1:2) | 166.1 ± 8.5 | 0.09 ± 0.05 | −48.0 ± 6.0 | 16.0 ± 8.5 | Lo |
| DSPC:DPPG:CHOL (4:1:2) | 177.3 ± 6.6 | 0.08 ± 0.03 | −46.4 ± 9.5 | 15.8 ± 5.5 | Lo |
| DPPC:DPPG:CHOL (4:1:2) | 173.5 ± 10.6 | 0.08 ± 0.04 | −46.2 ± 11.7 | 24.7 ± 10.2 | Lo |
| DSPC:DOPG:CHOL (4:1:2) | 168.1 ± 17.0 | 0.10 ± 0.05 | −45.8 ± 4.9 | 13.9 ± 3.9 | Lo |
| DOPC:DOPG:CHOL (4:1:2) | 158.7 ± 14.7 | 0.12 ± 0.03 | −43.4 ± 5.1 | 24.8 ± 12.8 | Lo |
| DSPC:DSPG (4:1) | 138.4 ± 13.2 | 0.10 ± 0.03 | −39.7 ± 5.7 | 11.4 ± 6.2 | Gel |
| DOPC:DOPG (4:1) | 140.1 ± 4.9 | 0.13 ± 0.03 | −44.9 ± 5.9 | 24.6 ± 12.9 | Ld |

[a] Percentage of $OVA_{323}$ amount remaining in liposomes after purification compared to the initial amount. Lo = Liquid ordered, Ld = liquid disordered.

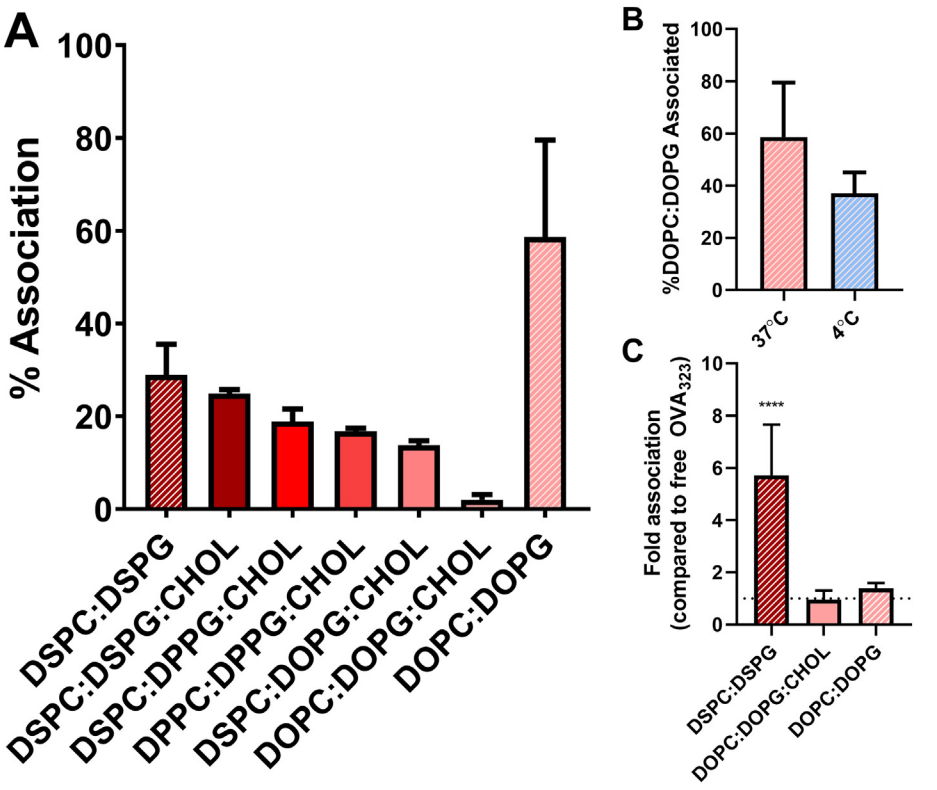


**Fig. 2.** Liposomal association (uptake and/or adsorption) by BMDCs *in vitro*. (A) $OVA_{323}$-containing fluorescently labeled liposomes were incubated for 4 h with BMDCs at 37 °C. Liposomes were subsequently washed away and cells were incubated overnight before being analyzed *via* flow cytometry. % Association indicates the percentage of live BMDCs that are positive for the fluorescent label in the liposomes. (B) Association of $OVA_{323}$-containing fluorescently labeled DOPC:DOPG liposomes at 37 °C *vs.* 4 °C. (C) Association of encapsulated $OVA_{323}$ to BMDCs. Fluorescently labeled $OVA_{323}$ was encapsulated in liposomes and incubated for 4 h with BMDCs at 37 °C. Liposomes were subsequently washed away and cells were incubated overnight before being analyzed by flow cytometry. Association was normalized to % of BMDCs positive for fluorescently labeled $OVA_{323}$ in the free $OVA_{323}$ control. Graphs show mean ± SD, (A) $n = 3$, (B) $n = 9$, (C) $n = 6$. $^{****}p < .0001$, compared to free $OVA_{323}$ determined by one-way ANOVA and Bonferroni's multiple comparisons test.

induction *in vivo*. An adoptive transfer mouse model using ovalbumin-specific OT-II T cells was used to study the induction of antigen-specific Treg responses by the liposomes *in vivo*. We selected the highest rigidity (DSPC:DSPG) and lowest rigidity liposomes (DOPC:DOPG) and their CHOL-containing counterparts. Both DSPC:DSPG and DSPC:DSPG:CHOL liposomes showed a significantly higher expansion of antigen-specific $CD4^+$ T cells than the formulations containing DOPC and DOPG (DSPC:DSPG 7.3 ± 0.9%, DSPC:DSPG:CHOL 7.3 ± 2.6%, DOPC:DOPG:CHOL 4.1 ± 0.3%, and DOPC:DOPG 4.1 ± 0.7%, Fig. 4A, B, C, D, and E). Moreover, in line with the *in vitro* results, the

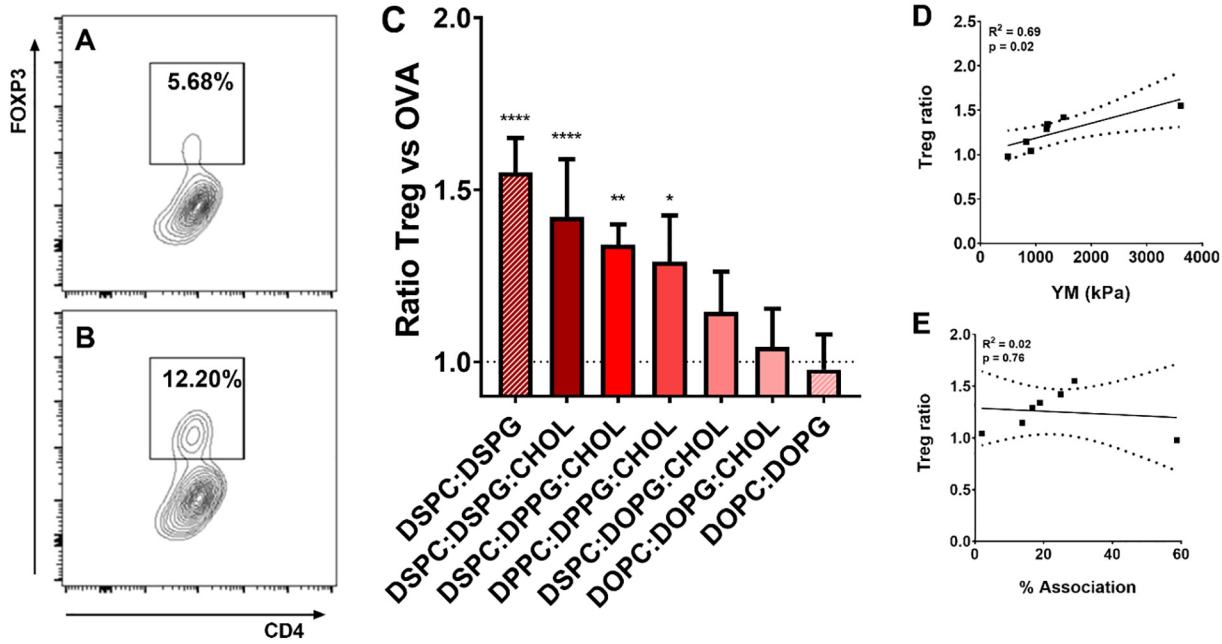


**Fig. 3.** Induction of Tregs by $OVA_{323}$-loaded liposomes *in vitro*. BMDCs were pulsed for 4 h with liposomes or controls and subsequently co-cultured for 72 h with $CD4^+$ T cells isolated from OT-II splenocytes. Flow cytometry was used to measure $FOXP3^+Ki\text{-}67^+CD4^+$ T cells. Representative flow cytometry plots of $FOXP3^+CD4^+$ T cells in the live $Ki\text{-}67^+CD4^+$ T cell population of OT-II T cells cultured with (A) free $OVA_{323}$ (0.1 μg/mL) and (B) $OVA_{323}$-loaded DSPC:DSPG liposomes (0.1 μg/mL $OVA_{323}$). (C) Summary Treg data of all liposomal formulations tested. Results were normalized to % $FOXP3^+Ki\text{-}67^+CD4^+$ T cells in the free $OVA_{323}$ control. The dashed line at Y = 1 represents the free $OVA_{323}$ control. Graph shows mean ± SD, $n = 4$. Linear correlations (95% CI) between (D) YM and Treg response ratio, and (E) % association and Treg response ratio. $^{****}p < .0001$, $^{**}p < .01$. $^{*}p < .05$, compared to free $OVA_{323}$ determined by one-way ANOVA and Bonferroni's multiple comparisons test.

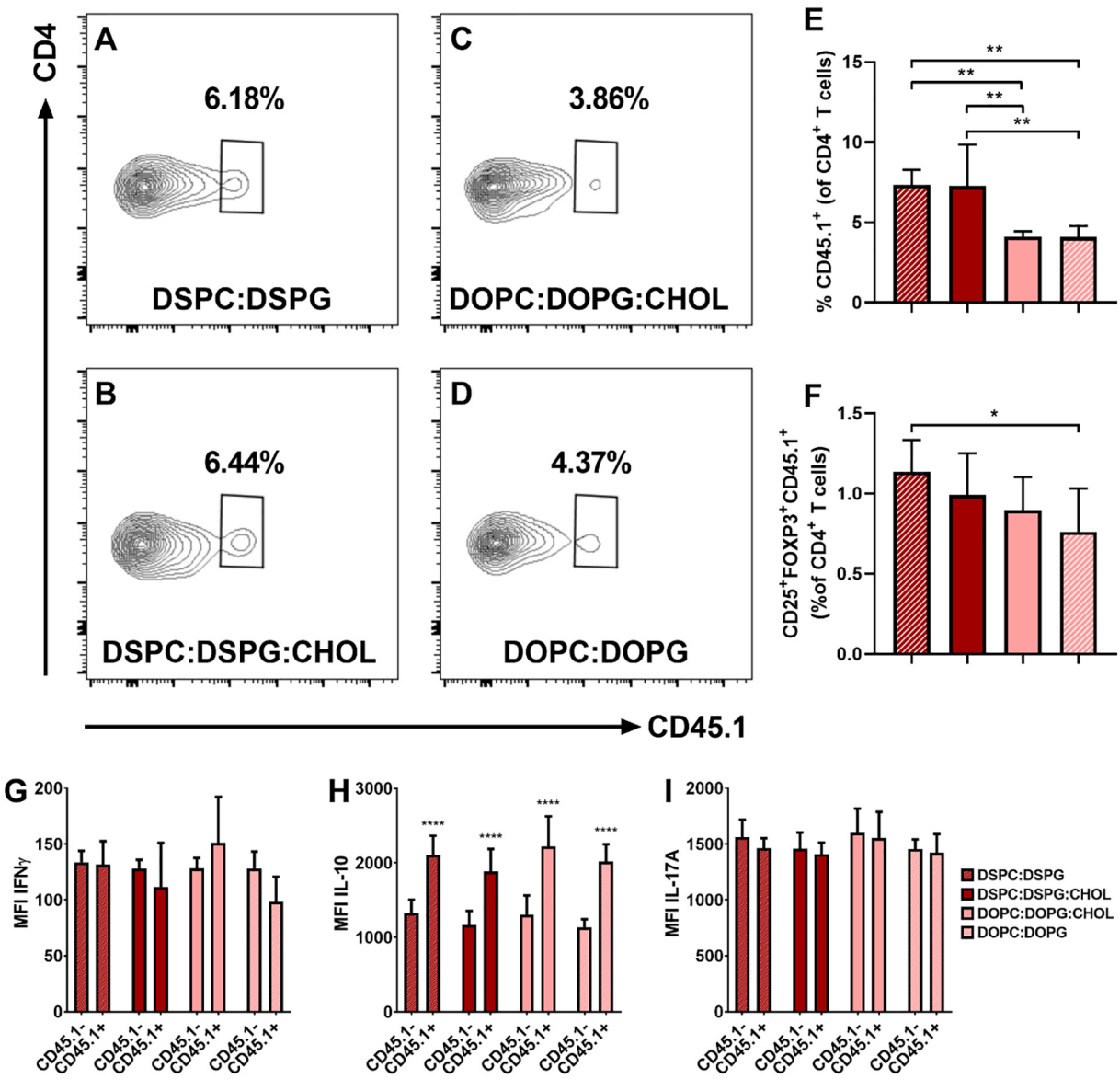


**Fig. 4.** Expansion of $OVA_{323}$ -specific Tregs in spleens of mice 8 days after i.v. injection of $OVA_{323}$-containing liposomes. Representative flow cytometry plots of $OVA_{323}$-specific $CD45.1^+CD4^+$ T cells in the spleen of a mouse injected with (A) DSPC:DSPG, (B) DSPC:DSPG:CHOL, (C) DOPC:DOPG:CHOL and (D) DOPC:DOPG liposomes containing $OVA_{323}$. (E) Percentage of $CD45.1^+$ cells in the $CD4^+$ T cell population. (F) % of $CD25^+FOXP3^+CD45.1^+$ Tregs in the $CD4^+$ T cell population. Graphs show mean ± SD, $n = 8$. $^*p < .05$, $^{**}p < .01$, compared to free $OVA_{323}$ determined by one-way ANOVA and Bonferroni's multiple comparisons test. Intracellular (G) IFNγ, (H) IL-10, and (I) IL-17A staining in splenocytes restimulated with 10 μg/mL OVA323 peptide for 6 h. $^{****}p < .0001$ comparing $CD45.1^+CD4^+$ T cells to $CD45.1^+CD4^+$ T cells. No significant differences found between liposomal formulations as measured by two way ANOVA with Bonferroni's post-test.

total percentage of antigen-specific Tregs within the $CD4^+$ T cell population was highest for DSPC:DSPG liposomes, and decreased with decreasing liposome rigidity (Fig. 4F). We observed no differences in Th1 and Th2 responses between liposomal formulations (Fig. S3). Furthermore, there were no differences in the production of IFNγ, IL-10 and IL-17A by splenocytes between liposomal formulations upon restimulation with $OVA_{323}$ for 6 h (Fig. 4G, H and I), although we did find a significant increase in production of IL-10 in all groups comparing antigen-specific $CD4^+$ T cells to $CD45.1^-CD4^+$ T cells, suggesting liposomal vaccination induces functional Tregs.

## 4. Discussion

The induction of antigen-specific Tregs through vaccination is an attractive approach for the treatment of autoimmune diseases. We and others have previously shown that nanoparticles, such as liposomes, can be used to induce these Tregs [10,13]. Generally, approaches to optimize such nanoparticles are focused on studying the effect of particle size and surface charge, while another important parameter, rigidity, is often overlooked [15]. This parameter is usually approximated by the phase properties of the lipid bilayers by analytical techniques such as DSC and Laurdan anisotropy. Besides the fact that these techniques only provide information about the bilayer of liposomes and thereby exclude other influencing factors, such as size, lamellarity, antigen content, and formulation excipients, there are other issues associated with these techniques. For instance, many liposomal formulations contain CHOL in the lipid bilayer, which compromises the suitability of techniques such as DSC [25], Fourier-transform infrared spectroscopy (FTIR) [36], and Laurdan anisotropy [37]. Furthermore, compounds encapsulated in liposomes can also interfere with DSC

[38,39] and FTIR measurements [40]. Other analytical techniques such as measuring the ability of particles to be extruded [41,42] are indirect measurements of rigidity. Importantly, all of the aforementioned techniques can only measure the average properties of a batch of particles. In contrast, AFM is an excellent technique to accurately measure the rigidity of individual particles and is not hindered by the presence of other compounds, such as CHOL and antigen. To further confirm this, studies should be performed to compare AFM to other techniques that measure liposomal rigidity.

We observed that CHOL reduces DSPC:DSPG liposome rigidity, and increases DOPC:DOPG liposome rigidity. The lipid bilayers of liposomes can generally be classified into three physical states with increasing rigidity: liquid disordered (bilayers composed of low-$T_m$ phospholipids), liquid ordered (bilayers composed of high- or low-$T_m$ phospholipids containing at least 20 mol% CHOL) and gel state (bilayers containing high-$T_m$ phospholipids). In the gel state, CHOL disrupts the tight packing of the lipids, while in the liquid disordered state, CHOL occupies space at the interfacial region near the membrane surface and replaces the hydrated $CH_2$ groups. As the acyl chains become dehydrated and straighten out, the packing becomes tighter and rigidity is therefore increased [43]. While bilayer state is not the same as liposomal rigidity, it is most likely one of the most important parameters that influence the rigidity of the liposomes. This is also in line with results from Takechi-Haraya et al. who used AFM to study the effect of CHOL on liposome rigidity [44].

From our study, it became clear that the introduction of lipid order mismatch significantly affects the rigidity of the liposomes. Mixing of lipids with different phase transitions in the absence of CHOL can lead to the formation of lipid domains (*e.g.* rigid domains and fluid domains), which could destabilize the bilayer packing, and thereby the rigidity of the liposomes [23]. We observed a significant decrease in rigidity of liposomes in the presence of a small amount of lower-$T_m$ lipid (*e.g.* DSPC:DSPG:CHOL *vs.* DSPC:DPPG:CHOL, Table S3), which did not further decrease upon complete substitution (*e.g.* DSPC:DPPG:CHOL *vs.* DPPC:DPPG:CHOL). This suggests that the $T_m$ values and the molar ratio of the constituent lipids are poor predictors of the rigidity of the liposomes (Fig. S1).

Physicochemical properties of liposomes other than bilayer composition can also affect their rigidity. For example, smaller liposomes, measured by AFM, are more rigid than larger liposomes [45]. This may be due to the different curvature of liposomes of different sizes, leading to more restricted molecular interactions between the lipids of smaller liposomes [46]. The charge of liposomes can also affect rigidity

neutral DOPC liposomes measured by AFM were shown to be more rigid than anionic DOPC:DOPG or cationic DOPC:DOTAP liposomes. This was hypothesized to be due to electrostatic repulsions causing structural destabilization of the lipid bilayer [47]. Due to technical limitations, the AFM measurements were performed at 25 °C. Since temperature affects the phase state of the lipid bilayers, it also influences the rigidity of liposomes. However, the phase states of the used phospholipids are the same at 25 °C and 37 °C (Table S1), so the trends in YM at this physiologically more relevant temperature should be very similar to those observed at 25 °C. Furthermore, a recent study found no difference in anionic liposome stiffness over the temperature range of 25–37 °C [48]. Finally, antigen content may affect liposomal rigidity. In this study, we have generated liposomal formulations with similar size, antigen loading, and ζ-potential to allow an *in vitro* and *in vivo* assessment primarily based on liposome rigidity.

The liposomes we measured had a range of YM from about 500 kPa to almost 4 MPa (Fig. 1B). For comparison, the YM of most mammalian cells was measured to be between 0.02 and 400 kPa [49] and that of cortical bone was reported to be about 20 GPa [50]. Moreover, we have used our AFM method to measure other anionic particle type, PLGA nanoparticles (*Z*-average diameter of 142.1 ± 1.1 nm, PDI of 0.073 ± 0.016, ζ-potential −49.7 ± 4.2 mV), which had a YM of 14.4 MPa ± 1.8 MPa. This illustrates that the range of rigidities of the liposomes is relatively small. This is especially true for the CHOL-containing liposomes, the rigidity of which ranged from about 800 kPa to 1500 kPa (Fig. 1B). This was expected since their bilayers are all in the liquid disordered state. However, even such small differences in rigidity could be measured using our AFM method, and we could measure significant differences between formulations (Table S3), illustrating the strength of this technique.

We have reported the SD of YM values of all liposomes measured within a batch. The SD of YM was relatively high for each liposomal formulation. The high SD was not due to a lack of precision of the AFM measurements, as repeated measurements of the same liposomes showed very low variation (the difference between two measurements of the same DSPC:DSPG:CHOL:$OVA_{323}$ liposomes was 2.8%, Table S4). Rather, it illustrates the variation in YM of the liposomes within a formulation, which is likely due to differences in size, lamellarity, and possibly antigen loading among different individual liposomes within the same batch. Variation in YM as measured in two different batches of DSPC:DSPG:CHOL:$OVA_{323}$ liposomes was also very low (1467 ± 575 kPa *vs.* 1510 ± 514, Fig. S4).

Based on previous reports we expected that the rigidity of the liposomes would positively correlate with their uptake by APCs since it requires less energy for a cell membrane to wrap around rigid particles [51]. It is known that phospholipid saturation has a significant effect on their fate in biological systems. For instance, dimethyldioctadecylammonium:trehalose 6,6′-dibehenate (DDA:TDB) liposomes showed higher retention at the site of injection and uptake by APCs *in vivo* compared to more fluid (as measured by DSC) dimethyldioleoylammonium (DODA):TDB liposomes [18]. Furthermore, CHOL content negatively correlated with uptake by THP-1-derived macrophages [52]. In our study, almost all formulations show a positive trend between liposomal rigidity and APC association. However, DOPC:DOPG liposomes showed the highest association to BMDCs of all tested formulations (Fig. 2A), which was not expected since these liposomes presented the lowest rigidity (Fig. 1B). Their route of uptake could be different from that of the more rigid formulations. For instance, pure DOPC liposomes (YM of 45 kPa as measured by AFM) were hypothesized to fuse with cells [53]. The DOPC:DOPG liposomes showed high passive association (Fig. 2B), and did not deliver their cargo to BMDCs (Fig. 2C), explaining their inability to induce T cell responses (Fig. 3C). There is evidence of an inverse relationship between liposomal rigidity and membrane permeability, as measured by calcein leakage [37]. So, it may be that the peptide had leaked out of the DOPC:DOPG and DOPC:DOPG:CHOL liposomes prior to BMDC association. This hypothesis is supported by our observation that a mixture of free $OVA_{323}$ and empty DOPC:DOPG or DOPC:DOPG:CHOL liposomes showed the same amount of $OVA_{323}$ association as encapsulated peptide (data not shown). Since we used fluorescently-labeled lipids and peptides, we cannot exclude the influence of the fluorophore itself on the measured association in BMDCs. However, since all formulations (aside from DOPC:DOPG liposomes) show almost no association of fluorophore when incubated at 4 °C (Fig. S2), the fluorophore itself likely has no effect on association.

We observed a clear correlation between the rigidity of the liposomes and the Treg responses they elicited *in vitro* and *in vivo* (Figs. 3D, 4F). While others have shown a link between increased rigidity and MHC-II presentation [19], and enhanced humoral and cellular responses [54,55], we are the first to report the effects of rigidity on Treg responses. This may have implications for the design of delivery systems aimed to enhance antigen-specific Treg responses.

In conclusion, we showed that liposomal rigidity as measured by our optimized AFM method is an important parameter in eliciting antigen-specific Treg responses *in vitro* and *in vivo*. Our findings may contribute to a better understanding of the factors driving Treg responses. Moreover, this paper may contribute to a rational design of liposomal as well as other nanoparticulate vaccine formulations aiming to enhance antigen-specific Treg responses for the treatment of autoimmune

diseases.

## Author contributions

N.B., B.S., J.K., and W.J. conceived of the experiments. N.B., R.J.T.L., M.G., J.v.D., F.L.V., and M.A.N. carried out the experiments and analyzed the data. F.G. provided support during AFM experiments and S.R. provided support with UPLC and HPLC. N.B. wrote the manuscript with support from all co-authors. The authors declare no competing financial interests.

## Funding sources

This work was supported by the Netherlands CardioVascular Research Initiative: the Dutch Heart Foundation, Dutch Federation of University Medical Centers, the Netherlands Organization for Health Research and Development, and the Royal Netherlands Academy of Sciences for the GENIUS project “Generating the best evidence-based pharmaceutical targets for atherosclerosis” (CVON2011-19).

## Appendix A. Supplementary data

Supplementary data to this article can be found online at https://doi.org/10.1016/j.jconrel.2019.12.003.

## References

[1] S. Sakaguchi, et al., Regulatory T cells and immune tolerance, Cell 133 (5) (2008) 775–787.
[2] Z. Mallat, H. Ait-Oufella, A. Tedgui, Regulatory T-cell immunity in atherosclerosis, Trends Cardiovasc. Med. 17 (4) (2007) 113–118.
[3] C. Keijzer, et al., Treg inducing adjuvants for therapeutic vaccination against chronic inflammatory diseases, Front. Immunol. 4 (2013) 245.
[4] M. Dominguez-Villar, D.A. Hafler, Regulatory T cells in autoimmune disease, Nat. Immunol. 19 (7) (2018) 665–673.
[5] A.M. Faria, H.L. Weiner, Oral tolerance: therapeutic implications for autoimmune diseases, Clin. Dev. Immunol. 13 (2–4) (2006) 143–157.
[6] T.K. Kishimoto, R.A. Maldonado, Nanoparticles for the induction of antigen-specific immunological tolerance, Front. Immunol. 9 (2018) 230.
[7] M.S. Macauley, et al., Antigenic liposomes displaying CD22 ligands induce antigen-specific B cell apoptosis, J. Clin. Invest. 123 (7) (2013) 3074–3083.
[8] L. Pang, et al., Encapsulating an immunosuppressant enhances tolerance induction by Siglec-engaging Tolerogenic liposomes, Chembiochem 18 (13) (2017) 1226–1233.
[9] R.A. Maldonado, et al., Polymeric synthetic nanoparticles for the induction of antigen-specific immunological tolerance, Proc. Natl. Acad. Sci. U. S. A. 112 (2) (2015) E156–E165.
[10] S. Rodriguez-Fernandez, et al., Phosphatidylserine-liposomes promote Tolerogenic features on dendritic cells in human type 1 diabetes by apoptotic mimicry, Front. Immunol. 9 (2018) 253.
[11] D.S. Watson, A.N. Endsley, L. Huang, Design considerations for liposomal vaccines: influence of formulation parameters on antibody and cell-mediated immune responses to liposome associated antigens, Vaccine 30 (13) (2012) 2256–2272.
[12] Z. Hunter, et al., A biodegradable nanoparticle platform for the induction of antigen-specific immune tolerance for treatment of autoimmune disease, ACS Nano 8 (3) (2014) 2148–2160.
[13] N. Benne, et al., Anionic 1,2-distearoyl-sn-glycero-3-phosphoglycerol (DSPG) liposomes induce antigen-specific regulatory T cells and prevent atherosclerosis in mice, J. Control. Release 291 (2018) 135–146.
[14] M.F. Bachmann, G.T. Jennings, Vaccine delivery: a matter of size, geometry, kinetics and molecular patterns, Nat. Rev. Immunol. 10 (11) (2010) 787–796.
[15] N. Benne, et al., Orchestrating immune responses: how size, shape and rigidity affect the immunogenicity of particulate vaccines, J. Control. Release 234 (2016) 124–134.
[16] A.C. Anselmo, S. Mitragotri, Impact of particle elasticity on particle-based drug delivery systems, Adv. Drug Deliv. Rev. 108 (2017) 51–67.
[17] K.A. Beningo, Y.L. Wang, Fc-receptor-mediated phagocytosis is regulated by mechanical properties of the target, J. Cell Sci. 115 (4) (2002) 849–856.
[18] D. Christensen, et al., A cationic vaccine adjuvant based on a saturated quaternary ammonium lipid have different in vivo distribution kinetics and display a distinct CD4 T cell-inducing capacity compared to its unsaturated analog, J. Control. Release 160 (3) (2012) 468–476.
[19] K. Norling, et al., Gel phase 1,2-Distearoyl-sn-glycero-3-phosphocholine-based liposomes are superior to fluid phase liposomes at augmenting both antigen presentation on major histocompatibility complex class II and Costimulatory molecule display by dendritic cells in vitro, ACS Infect. Dis. 5 (11) (2019) 1867–1878.
[20] T. Yasuda, G.F. Dancey, S.C. Kinsky, Immunogenicity of liposomal model membranes in mice: dependence on phospholipid composition, Proc. Natl. Acad. Sci. U. S. A. 74 (3) (1977) 1234–1236.
[21] G.F. Dancey, T. Yasuda, S.C. Kinsky, Effect of liposomal model membrane composition on immunogenicity, J. Immunol. 120 (4) (1978) 1109–1113.
[22] O. Bakouche, D. Gerlier, Enhancement of immunogenicity of tumour virus antigen by liposomes: the effect of lipid composition, Immunology 58 (3) (1986) 507–513.
[23] O.G. Mouritsen, K. Jorgensen, Dynamical order and disorder in lipid bilayers, Chem. Phys. Lipids 73 (1–2) (1994) 3–25.
[24] C. Demetzos, Differential scanning Calorimetry (DSC): a tool to study the thermal behavior of lipid bilayers and liposomal stability, J. Liposome. Res. 18 (3) (2008) 159–173.
[25] C. Matsingou, C. Demetzos, Calorimetric study on the induction of interdigitated phase in hydrated DPPC bilayers by bioactive labdanes and correlation to their liposome stability: The role of chemical structure, Chem. Phys. Lipids 145 (1) (2007) 45–62.
[26] E. Spyratou, et al., Atomic force microscopy: a tool to study the structure, dynamics and stability of liposomal drug delivery systems, Expert Opin. Drug. Deliv. 6 (3) (2009) 305–317.
[27] E.M. Varypataki, et al., Efficient eradication of established Tumors in mice with cationic liposome-based synthetic long-peptide vaccines, Cancer Immunol. Res. 5 (3) (2017) 222–233.
[28] V. Filipe, A. Hawe, W. Jiskoot, Critical evaluation of nanoparticle tracking analysis (NTA) by NanoSight for the measurement of nanoparticles and protein aggregates, Pharm. Res. 27 (5) (2010) 796–810.
[29] E.M. Varypataki, et al., Cationic liposomes loaded with a synthetic long peptide and poly(I:C): a defined adjuvanted vaccine for induction of antigen-specific T cell cytotoxicity, AAPS J. 17 (1) (2015) 216–226.
[30] K. van der Maaden, et al., Fluorescent nanoparticle adhesion assay: a novel method for surface pKa determination of self-assembled monolayers on silicon surfaces, Langmuir 28 (7) (2012) 3403–3411.
[31] J.A. Howarter, J.P. Youngblood, Optimization of silica silanization by 3-aminopropyltriethoxysilane, Langmuir 22 (26) (2006) 11142–11147.
[32] A.A. Duarte, et al., Adsorption kinetics of DPPG liposome layers: a quantitative analysis of surface roughness, Microsc. Microanal. 19 (4) (2013) 867–875.
[33] Determining the elastic modulus of biological samples using atomic force microscopy. JPK Instruments AG Application Note. p. 1–9.
[34] D.C. Lin, E.K. Dimitriadis, F. Horkay, Robust strategies for automated AFM force curve analysis–I. non-adhesive indentation of soft, inhomogeneous materials, J. Biomech. Eng. 129 (3) (2007) 430–440.
[35] X. Liang, G. Mao, K.Y. Simon Ng, Probing small unilamellar EggPC vesicles on mica surface by atomic force microscopy, Colloids Surf. B: Biointerfaces 34 (1) (2004) 41–51.
[36] C. Altunayar, I. Sahin, N. Kazanci, A comparative study of the effects of cholesterol and desmosterol on zwitterionic DPPC model membranes, Chem. Phys. Lipids 188 (2015) 37–45.
[37] Y. Takechi-Haraya, K. Sakai-Kato, Y. Goda, Membrane rigidity determined by atomic force microscopy is a parameter of the permeability of liposomal membranes to the hydrophilic compound Calcein, AAPS PharmSciTech 18 (5) (2017) 1887–1893.
[38] L. Zhao, et al., DSC and EPR investigations on effects of cholesterol component on molecular interactions between paclitaxel and phospholipid within lipid bilayer membrane, Int. J. Pharm. 338 (1–2) (2007) 258–266.
[39] J.O. Eloy, et al., Co-loaded paclitaxel/rapamycin liposomes: development, characterization and in vitro and in vivo evaluation for breast cancer therapy, Colloids Surf. B: Biointerfaces 141 (2016) 74–82.
[40] N. Toyran, F. Severcan, Interaction between vitamin D2 and magnesium in liposomes: differential scanning calorimetry and FTIR spectroscopy studies, J. Mol. Struct. 839 (1–3) (2007) 19–27.
[41] B.A. van den Bergh, et al., Elasticity of vesicles assessed by electron spin resonance, electron microscopy and extrusion measurements, Int. J. Pharm. 217 (1–2) (2001) 13–24.
[42] J.W. Myerson, et al., Flexible Nanoparticles Reach Sterically Obscured Endothelial Targets Inaccessible to Rigid Nanoparticles, Adv. Mater. 30 (32) (2018) e1802373.
[43] M.R. Krause, S.L. Regen, The structural role of cholesterol in cell membranes: from condensed bilayers to lipid rafts, Acc. Chem. Res. 47 (12) (2014) 3512–3521.
[44] Y. Takechi-Haraya, et al., Atomic force microscopic analysis of the effect of lipid composition on liposome membrane rigidity, Langmuir 32 (24) (2016) 6074–6082.
[45] N. Delorme, A. Fery, Direct method to study membrane rigidity of small vesicles based on atomic force microscope force spectroscopy, Phys. Rev. E Stat. Nonlinear Soft Matter Phys. 74 (3 Pt 1) (2006) 30901.
[46] K. Nakano, et al., A novel method for measuring rigidity of submicron-size liposomes with atomic force microscopy, Int. J. Pharm. 355 (1–2) (2008) 203–209.
[47] Y. Takechi-Haraya, Y. Goda, K. Sakai-Kato, Atomic force microscopy study on the stiffness of Nanosized liposomes containing charged lipids, Langmuir 34 (26) (2018) 7805–7812.
[48] Y. Takechi-Haraya, et al., Improved atomic force microscopy stiffness measurements of Nanoscale liposomes by cantilever tip shape evaluation, Anal. Chem. 91 (16) (2019) 10432–10440.
[49] T.G. Kuznetsova, et al., Atomic force microscopy probing of cell elasticity, Micron 38 (8) (2007) 824–833.
[50] J.Y. Rho, R.B. Ashman, C.H. Turner, Young’s modulus of trabecular and cortical bone material: ultrasonic and microtensile measurements, J. Biomech. 26 (2) (1993) 111–119.
[51] X. Yi, X. Shi, H. Gao, Cellular uptake of elastic nanoparticles, Phys. Rev. Lett. 107 (9) (2011) 098101.
[52] R. Kaur, et al., Effect of incorporating cholesterol into DDA:TDB liposomal

adjuvants on bilayer properties, biodistribution, and immune responses, Mol. Pharm. 11 (1) (2014) 197–207.
[53] P. Guo, et al., Nanoparticle elasticity directs tumor uptake, Nat. Commun. 9 (1) (2018) 130.
[54] F. Garnier, et al., Enhancement of in vivo and in vitro T cell response against measles virus haemagglutinin after its incorporation into liposomes: effect of the phospholipid composition, Vaccine 9 (5) (1991) 340–345.
[55] T. Mazumdar, K. Anam, N. Ali, Influence of phospholipid composition on the adjuvanticity and protective efficacy of liposome-encapsulated Leishmania donovani antigens, J. Parasitol. 91 (2) (2005) 269–274.